

$c \rightarrow u\bar{\nu}$ transitions of B_c mesons: 331 model facing Standard Model null tests

Pietro Colangelo^{1,*}, Fulvia De Fazio^{1,†} and Francesco Loparco^{1,2,‡}

¹*Istituto Nazionale di Fisica Nucleare, Sezione di Bari, via Orabona 4, 70126 Bari, Italy*

²*Dipartimento Interateneo di Fisica “Michelangelo Merlin”, Università degli Studi di Bari, via Orabona 4, 70126 Bari, Italy*



(Received 19 July 2021; accepted 29 November 2021; published 22 December 2021)

The Glashow-Iliopoulos-Maiani mechanism is extremely efficient to suppress the flavor-changing neutral current decays of charmed hadrons induced by the $c \rightarrow u$ transitions, making such processes particularly sensitive to phenomena beyond the Standard Model. In particular, $c \rightarrow u$ decays with a neutrino pair in the final state are theoretically appealing due to the small long-distance contributions. Moreover, in the framework of the Standard Model effective field theory (SMEFT), the $SU(2)_L$ invariance allows us to relate the Wilson coefficients in the effective Hamiltonian governing the $c \rightarrow u\bar{\nu}$ decays to the coefficients in the $c \rightarrow u\ell^+\ell^-$ Hamiltonian. We analyze the $B_c \rightarrow B^{(*)+}\nu\bar{\nu}$ decays, for which branching fractions of at most $\mathcal{O}(10^{-16})$ are predicted in the Standard Model including short- and long-distance contributions, so small that they can be considered as null tests. Using SMEFT and the relation to the $c \rightarrow u\ell^+\ell^-$ processes, we study the largest enhancement achievable in generic new physics scenarios, then we focus on a particular extension of the Standard Model, the 331 model. SMEFT relations and the connection with $c \rightarrow u\ell^+\ell^-$ imply that $\mathcal{B}(B_c \rightarrow B^{(*)+}\nu\bar{\nu})$ could even reach $\mathcal{O}(10^{-6})$, an extremely large enhancement. A less pronounced effect is found in the 331 model, with $\mathcal{O}(10^{-11})$ predicted branching fractions. Within the 331 model, correlations exist among the $B_c \rightarrow B^{(*)+}\nu\bar{\nu}$ and $K \rightarrow \pi\nu\bar{\nu}$, $B \rightarrow (X_s, K, K^*)\nu\bar{\nu}$ channels.

DOI: [10.1103/PhysRevD.104.115024](https://doi.org/10.1103/PhysRevD.104.115024)

I. INTRODUCTION

In the Standard Model (SM), the flavor-changing neutral current (FCNC) transitions occur at loop level and are generally characterized by Cabibbo-Kobayashi-Maskawa (CKM) and loop suppressions. The CKM cancellation mechanism is particularly efficient in the processes involving up-type quarks which take place through penguin and box diagrams with internal down-type quark exchanges. This is the case of the charmed hadron decays induced by the $c \rightarrow u\ell^+\ell^-$ and $c \rightarrow u\bar{\nu}$ transitions, for which tiny branching fractions are predicted in SM considering the short-distance amplitude [1]. The modes with charged dileptons are polluted by long-distance (LD) hadronic contributions, and the phase-space regions where such terms are large must be cut to pin down the effects of the short-distance term [2]. In the $c \rightarrow u$ dineutrino modes,

long-distance effects are smaller than in the charged dilepton modes. Therefore, such processes represent genuine null tests of the SM; their observation would be an indication of phenomena beyond the Standard Model (BSM). Among all hadrons, the decays of B_c induced by the $c \rightarrow u$ transitions are particularly interesting, since in this case the main long-distance contributions affect a region of the phase-space near the end point, differently, e.g., from D , D_s , and Λ_c . Hence, B_c plays an important role in testing the Standard Model [3]. On general grounds, searching for new physics (NP) effects requires the analysis of several modes induced by the same underlying transition; the correlations among the various observables are important to identify the possible NP contributions and to relate them to the structure of the SM extensions.

The short-distance low-energy Hamiltonian governing the $c \rightarrow u\bar{\nu}$ transition has a simple structure. For left-handed neutrinos, it consists of two operators,

$$\mathcal{H}_{\text{eff}} = C_L \mathcal{Q}_L + C_R \mathcal{Q}_R, \quad (1)$$

with

$$\begin{aligned} \mathcal{Q}_L &= (\bar{u}\gamma^\mu(1-\gamma_5)c)(\bar{\nu}\gamma_\mu(1-\gamma_5)\nu), \\ \mathcal{Q}_R &= (\bar{u}\gamma^\mu(1+\gamma_5)c)(\bar{\nu}\gamma_\mu(1-\gamma_5)\nu). \end{aligned} \quad (2)$$

*pietro.colangelo@ba.infn.it

†fulvia.defazio@ba.infn.it

‡francesco.loparco1@ba.infn.it

Published by the American Physical Society under the terms of the [Creative Commons Attribution 4.0 International license](https://creativecommons.org/licenses/by/4.0/). Further distribution of this work must maintain attribution to the author(s) and the published article's title, journal citation, and DOI. Funded by SCOAP³.

In the SM, the Hamiltonian comprises only \mathcal{Q}_L . The Wilson coefficient C_L^{SM} is obtained from loop diagrams with down-type quark exchanges,

$$C_L^{\text{SM}} = -\frac{G_F}{\sqrt{2}} \frac{\alpha}{2\pi \sin^2 \theta_W} \sum_{q=d,s,b} \lambda^q X(x_q). \quad (3)$$

In (3), G_F is the Fermi constant, α the fine structure constant, θ_W the Weinberg angle, and $\lambda^q = V_{cq}^* V_{uq}$ with V_{ij} the CKM matrix elements. The Inami-Lim function $X(x_q)$, depending on $x_q = m_q^2/M_W^2$, can be found in [4]. The dominant contribution from the intermediate b quark provides $|C_L^{\text{SM}}| \simeq \mathcal{O}(10^{-13})$. Analogously, the transitions $s \rightarrow d\nu\bar{\nu}$ and $b \rightarrow (s, d)\nu\bar{\nu}$ are governed by a low-energy Hamiltonian with the structure of (1) and intermediate up-type quarks. BSM phenomena can manifest themselves through the enhancement of C_L and through the effects of the operator \mathcal{Q}_R .

FCNC dineutrino modes have been extensively studied in the case of strange and beauty quarks. The $K^+ \rightarrow \pi^+\nu\bar{\nu}$ and $K_L \rightarrow \pi^0\nu\bar{\nu}$ transitions are under strict theoretical control [4] and intense experimental scrutiny [5–7]. In the beauty sector, the modes $B \rightarrow K^{(*)}\nu\bar{\nu}$ have been theoretically investigated [8–19] and are within the reach of the present facilities [20–23].

As for the charm sector, a few studies have analyzed the FCNC dineutrino modes in the SM and BSM frameworks [24–27]. Here, we focus on $B_c \rightarrow B^{(*)}\nu\bar{\nu}$ decays, for which lattice QCD results for the hadronic form factors can be used [28], with a control of the theoretical uncertainty related to nonperturbative QCD quantities. From the experimental point of view, these modes will be accessible at high energy e^+e^- colliders, namely the planned Future Circular Collider FCC-ee machine running at the Z^0 peak. We proceed both in a model-independent way and in a defined BSM framework. In the next section, we apply the Standard Model effective field theory (SMEFT) to relate the Wilson coefficients in the low-energy $c \rightarrow u\nu\bar{\nu}$ Hamiltonian (1) to the coefficients in the $c \rightarrow u\ell^+\ell^-$ Hamiltonian, as done in [24,25]. This allows us to establish the largest enhancement for the B_c branching fractions achievable in a generic NP scenario, with the numerical results discussed in Sec. III. In Sec. IV, we focus on a definite NP model, the 331 model in four variants. We observe that in this framework it is possible to relate the charm to the strange and beauty quark sectors, and that the $c \rightarrow u$ processes can be constrained using bounds from $\Delta S = 2$ and $\Delta B = 2$ observables. The correlations among B_c and kaon and B meson dineutrino decays are described in Sec. VI. In the last section, we draw our conclusions.

II. RELATING THE $c \rightarrow u$ DINEUTRINO AND CHARGED DILEPTON MODES USING SMEFT

A relation between the $c \rightarrow u$ dineutrino and the $c \rightarrow u$ charged dilepton modes can be established on the basis of

$SU(2)_L$ invariance using the Standard Model effective theory [24,25]. Considering the possibility of lepton flavor violation, one focuses on $c \rightarrow u\nu_i\bar{\nu}_j$ transitions, with the indices i, j denoting the neutrino flavors. The coefficients C_L and C_R in the low-energy Hamiltonian (1) become lepton-flavor dependent $C_{L,R}^{i,j}$ and can be combined giving

$$x_U^\pm = \sum_{i,j=1,2,3} |\tilde{C}_L^{i,j} \pm \tilde{C}_R^{i,j}|^2 \quad (4)$$

and

$$x_U = \frac{x_U^+ + x_U^-}{2}, \quad (5)$$

with $\tilde{C}_{L,R}$ defined by $C_{L,R} = -\frac{G_F}{\sqrt{2}} \frac{\alpha}{4\pi} \tilde{C}_{L,R}$. The combinations (4) and (5) account for the contributions of both the operators \mathcal{Q}_L and \mathcal{Q}_R .

The relation of $C_{L,R}$ to the Wilson coefficients in the $c \rightarrow u\ell^+\ell^-$ low-energy Hamiltonian has been proposed in [24,25]. For two generic quarks q_1 and q_2 , the $q_1 \rightarrow q_2\ell^+\ell^-$ general Hamiltonian reads [29]

$$H_{\text{eff}}^{q_1 \rightarrow q_2 \ell^+ \ell^-} = -4 \frac{G_F}{\sqrt{2}} \left[\sum_{i=9,10,S,P} (C_i \mathcal{Q}_i + C'_i \mathcal{Q}'_i) + C_T \mathcal{Q}_T + C_{T5} \mathcal{Q}_{T5} \right], \quad (6)$$

with the operators

$$\begin{aligned} \mathcal{Q}_9 &= \frac{\alpha}{4\pi} (\bar{q}_2 \gamma_\mu P_L q_1) (\bar{\ell} \gamma^\mu \ell), \\ \mathcal{Q}'_9 &= \frac{\alpha}{4\pi} (\bar{q}_2 \gamma_\mu P_R q_1) (\bar{\ell} \gamma^\mu \ell), \\ \mathcal{Q}_{10} &= \frac{\alpha}{4\pi} (\bar{q}_2 \gamma_\mu P_L q_1) (\bar{\ell} \gamma^\mu \gamma_5 \ell), \\ \mathcal{Q}'_{10} &= \frac{\alpha}{4\pi} (\bar{q}_2 \gamma_\mu P_R q_1) (\bar{\ell} \gamma^\mu \gamma_5 \ell), \\ \mathcal{Q}_S &= (\bar{q}_2 P_R q_1) (\bar{\ell} \ell), & \mathcal{Q}'_S &= (\bar{q}_2 P_L q_1) (\bar{\ell} \ell), \\ \mathcal{Q}_P &= (\bar{q}_2 P_R q_1) (\bar{\ell} \gamma_5 \ell), & \mathcal{Q}'_P &= (\bar{q}_2 P_L q_1) (\bar{\ell} \gamma_5 \ell), \\ \mathcal{Q}_T &= (\bar{q}_2 \sigma_{\mu\nu} q_1) (\bar{\ell} \sigma^{\mu\nu} \ell), \\ \mathcal{Q}_{T5} &= (\bar{q}_2 \sigma_{\mu\nu} q_1) (\bar{\ell} \sigma^{\mu\nu} \gamma_5 \ell), \end{aligned} \quad (7)$$

and $P_{R,L} = \frac{1 \pm \gamma_5}{2}$. The relations are obtained using the SMEFT operators classified in Ref. [30]. The tree-level matching of the dimension-6 four-fermion operators invariant under the SM $SU(3)_C \times SU(2)_L \times U(1)_Y$ gauge group with the Hamiltonian (1) gives the relations

$$C_L^{c \rightarrow u} = \frac{v^2}{2\Lambda^2} [(C_{lq}^{(1)} + C_{lq}^{(3)}) + (C_{\phi q}^{(1)} - C_{\phi q}^{(3)})],$$

$$C_R^{c \rightarrow u} = \frac{v^2}{2\Lambda^2} (C_{lu} + C_{\phi u}). \quad (8)$$

$C_{L,R}^{c \rightarrow u}$ are defined by $C_{L,R} = -\frac{G_F}{\sqrt{2}} C_{L,R}^{c \rightarrow u}$, with $C_{L,R}$ in (1). The operators corresponding to the coefficients in the rhs of Eq. (8) are expressed in the Warsaw basis [30]. In this equation, v is the electroweak vacuum expectation value and Λ the matching scale of NP with the SMEFT.

The relations between the coefficients in the $c \rightarrow u\ell^+\ell^-$ Hamiltonian (6) and the coefficients of the SMEFT operators can also be worked out,

$$C_9^{c \rightarrow u} = \frac{\pi v^2}{\alpha\Lambda^2} (C_{lq}^{(1)} - C_{lq}^{(3)} + C_{qe})$$

$$+ \frac{\pi v^2}{\alpha\Lambda^2} (-1 + 4s_W^2) (C_{\phi q}^{(1)} - C_{\phi q}^{(3)}),$$

$$C_9^{\prime c \rightarrow u} = \frac{\pi v^2}{\alpha\Lambda^2} (C_{eu} + C_{lu} + (-1 + 4s_W^2) C_{\phi u}),$$

$$C_{10}^{c \rightarrow u} = -\frac{\pi v^2}{\alpha\Lambda^2} (C_{lq}^{(1)} - C_{lq}^{(3)} - C_{qe}) + \frac{\pi v^2}{\alpha\Lambda^2} (C_{\phi q}^{(1)} - C_{\phi q}^{(3)}),$$

$$C_{10}^{\prime c \rightarrow u} = \frac{\pi v^2}{\alpha\Lambda^2} (C_{eu} - C_{lu} + C_{\phi u}),$$

$$C_S^{c \rightarrow u} = C_P^{c \rightarrow u} = -\frac{v^2}{4\Lambda^2} C_{lequ}^{(1)},$$

$$C_S^{\prime c \rightarrow u} = -C_P^{\prime c \rightarrow u} = -\frac{v^2}{4\Lambda^2} C_{lequ}^{(1)*},$$

$$C_T^{c \rightarrow u} = -\frac{v^2}{4\Lambda^2} 2\text{Re}[C_{lequ}^{(3)}],$$

$$C_{T5}^{c \rightarrow u} = -\frac{v^2}{4\Lambda^2} 2i\text{Im}[C_{lequ}^{(3)}]. \quad (9)$$

The SMEFT operators have generation indices. The coefficients in the rhs of Eqs. (8) and (9) read $C = C_{ij12}$, with i and j the lepton generation indices and 1,2 indicating the u and c quark in the first and second generation.¹

The coefficients of the SMEFT operators appearing in the rhs of Eq. (8) are also comprised in the rhs of Eq. (9). This allows us to translate the experimental bounds on the $c \rightarrow u\ell^+\ell^-$ modes, together with data on the $s \rightarrow d\ell^+\ell^-$ modes, into an upper bound for the combination x_U in Eq. (5) [24,25]. Indeed, the $SU(2)_L$ symmetry links the $c \rightarrow u\ell^+\ell^-$ with $c \rightarrow u\nu\bar{\nu}$ modes and the $s \rightarrow d\ell^+\ell^-$ with $c \rightarrow u\nu\bar{\nu}$ modes. The bound on x_U is obtained assuming conservatively that the experimental limits on the charged

¹In Ref. [31], the relations in Eq. (8) are obtained neglecting the contribution of the anomalous gauge boson couplings, which correspond to the SMEFT coefficients with indices ϕ . The relations for the $c \rightarrow u$ transitions are different from those for $b \rightarrow s$ [29].

dilepton branching fractions are saturated by the short-distance Hamiltonian (6). The limit depends on additional assumptions on the structure of the transitions; the most stringent one is obtained assuming lepton universality (LU) and charged lepton flavor conservation (cLFC) [24,25], with the results,

$$x_U \leq x_U^{\text{max}} = 34 \quad (\text{LU}), \quad (10)$$

$$x_U \leq x_U^{\text{max}} = 196 \quad (\text{cLFC}). \quad (11)$$

The bounds (10) and (11) have been considered in the analysis of D^\pm , D^0 , D_s , and charmed baryon decays induced by $c \rightarrow u\nu\bar{\nu}$ [24,25]. Here, we focus on $B_c^+ \rightarrow B^{(*)+\nu\bar{\nu}}$. We use the lattice QCD $B_c \rightarrow B_d$ form factors in [28] and the $B_c \rightarrow B_d^*$ form factors derived in [3] applying the heavy quark spin symmetry [32,33]. The $B_c^+ \rightarrow B^{(*)+}$ form factors are obtained invoking the isospin symmetry.

III. $B_c^+ \rightarrow B^{(*)+\nu\bar{\nu}}$ DECAYS

In the processes $B_c^+(p) \rightarrow B^+(p')\nu(k_1)\bar{\nu}(k_2)$ and $B_c^+(p) \rightarrow B^{*+}(p', \epsilon)\nu(k_1)\bar{\nu}(k_2)$, the particle momenta are p, p', k_1, k_2 , and ϵ is the B^* polarization vector. Denoting by E_{miss} the energy of the neutrino pair in the B_c rest frame, the dimensionless variable $x = \frac{E_{\text{miss}}}{m_{B_c}}$ varies in the range $\frac{1-r}{2} \leq x \leq 1 - \sqrt{r}$, with $r = \frac{m_{B^{(*)+}}^2}{m_{B_c}^2}$. The hadronic matrix elements in the decay amplitudes are parametrized in terms of form factors,

$$\langle B^+(p') | \bar{u}\gamma_\mu c | B_c(p) \rangle = f_+(q^2) \left(p_\mu + p'_\mu - \frac{m_{B_c}^2 - m_B^2}{q^2} q_\mu \right)$$

$$+ f_0(q^2) \frac{m_{B_c}^2 - m_B^2}{q^2} q_\mu \quad (12)$$

and

$$\langle B^{*+}(p', \epsilon) | \bar{u}\gamma_\mu c | B_c(p) \rangle = -\frac{2V(q^2)}{m_{B_c} + m_{B^*}} i\epsilon_{\mu\alpha\beta} \epsilon^{*\nu} p^\alpha p'^\beta,$$

$$\langle B^{*+}(p', \epsilon) | \bar{u}\gamma_\mu \gamma_5 c | B_c(p) \rangle$$

$$= (m_{B_c} + m_{B^*}) \left(\epsilon_\mu^* - \frac{(\epsilon^* \cdot q)}{q^2} q_\mu \right) A_1(q^2)$$

$$- \frac{(\epsilon^* \cdot q)}{m_{B_c} + m_{B^*}} \left((p + p')_\mu - \frac{m_{B_c}^2 - m_{B^*}^2}{q^2} q_\mu \right) A_2(q^2)$$

$$+ (\epsilon^* \cdot q) \frac{2m_{B^*}}{q^2} q_\mu A_0(q^2). \quad (13)$$

The $B_c^+ \rightarrow B^+\nu\bar{\nu}$ missing energy distribution obtained from (1) involves the form factor $f_+(q^2)$,

$$\frac{d\Gamma(B_c^+ \rightarrow B^+\nu\bar{\nu})}{dx} = 3 \frac{|C_L + C_R|^2 |f_+(q^2)|^2}{48\pi^3 m_{B_c}} \lambda^{3/2}(q^2, m_{B_c}^2, m_B^2), \quad (14)$$

with $q = p - p'$ and λ the Källén function. For $B_c^+ \rightarrow B^{*+}\nu\bar{\nu}$, the missing energy distributions for longitudinally and transversely polarized B^* read

$$\begin{aligned} \frac{d\Gamma_L}{dx} &= 3 \frac{|C_L - C_R|^2 |\vec{p}'|}{24\pi^3 m_{B^*}^2} ((m_{B_c} + m_{B^*})(m_{B_c} E' - m_{B^*}^2) A_1(q^2) - \frac{2m_{B_c}^2}{m_{B_c} + m_{B^*}} |\vec{p}'|^2 A_2(q^2))^2, \\ \frac{d\Gamma_{\pm}}{dx} &= 3 \frac{|\vec{p}'| q^2}{24\pi^3} \left| (C_L + C_R) \frac{2m_{B_c} |\vec{p}'|}{m_{B_c} + m_{B^*}} V(q^2) \mp (C_L - C_R)(m_{B_c} + m_{B^*}) A_1(q^2) \right|^2, \end{aligned} \quad (15)$$

with \vec{p}' and E' the B^* three-momentum and energy in the B_c rest frame. In Eqs. (14) and (15), the relation $q^2 = m_{B_c}^2(2x - 1) + m_{B^*}^2$ is used; the factor 3 is due to the sum over the three neutrino flavors.

As inferred from (14) and (15), $\mathcal{B}(B_c^+ \rightarrow B^+\nu\bar{\nu})$ depends on the combination x_U^+ in Eq. (4), $\mathcal{B}_L(B_c^+ \rightarrow B^{*+}\nu\bar{\nu})$ depends on x_U^- , and $\mathcal{B}_T(B_c^+ \rightarrow B^{*+}\nu\bar{\nu}) = \mathcal{B}_+(B_c^+ \rightarrow B^{*+}\nu\bar{\nu}) + \mathcal{B}_-(B_c^+ \rightarrow B^{*+}\nu\bar{\nu})$ depends on both combinations. Using

the parameters in Table I and the central values for the form factors [3,28] we obtain

$$\begin{aligned} \mathcal{B}(B_c^+ \rightarrow B^+\nu\bar{\nu}) &= 7.8 \times 10^8 |C_L + C_R|^2 \\ &= 6.9 \times 10^{-9} x_U^+ \end{aligned} \quad (16)$$

and

TABLE I. Parameters used in the analysis.

Constants and quark masses			
$G_F = 1.16637(1) \times 10^{-5} \text{ GeV}^{-2}$	[34]	$m_c(m_c) = 1.279(8) \text{ GeV}$	[35]
$M_W = 80.385(15) \text{ GeV}$	[34]	$m_b(m_b) = 4.163(16) \text{ GeV}$	[34,36]
$\sin^2 \theta_W = 0.23121(4)$	[34]	$m_t(m_t) = 162.5 \pm_{1.5}^{2.1} \text{ GeV}$	[34]
$\alpha(M_Z) = 1/127.9$	[34]	$M_t = 172.76(30) \text{ GeV}$	[34]
$\alpha_s^{(5)}(M_Z) = 0.1179(10)$	[34]		
Meson masses and lifetimes			
$m_{K^+} = 493.677(13) \text{ MeV}$	[34]	$\tau(K^+) = 1.2380(20) \times 10^{-8} \text{ s}$	[34]
$m_{K^0} = 497.611(13) \text{ MeV}$	[34]	$\tau(K_S) = 0.8954(4) \times 10^{-10} \text{ s}$	[34]
		$\tau(K_L) = 5.116(21) \times 10^{-8} \text{ s}$	[34]
$m_{B_d} = 5279.63(20) \text{ MeV}$	[34]	$\tau(B_d) = 1.519(4) \text{ ps}$	[34]
$m_{B^+} = 5279.25(26) \text{ MeV}$	[34]		
$m_{B^{*+}} = 5324.70(21) \text{ MeV}$	[34]		
$m_{B_s} = 5366.88(14) \text{ MeV}$	[34]	$\tau(B_s) = 1.515(4) \text{ ps}$	[34]
$m_{B_c} = 6274.9(8) \text{ MeV}$	[34]	$\tau(B_c) = 0.510(9) \text{ ps}$	[34]
Decay constants and parameters related to $\Delta F = 2$ observables			
$F_K = 156.1(11) \text{ MeV}$	[37]	$\hat{B}_K = 0.7625(97)$	[37]
$\Delta M_K = 0.5293(9) \times 10^{-2} \text{ ps}^{-1}$	[34]	$ \epsilon_K = 2.228(11) \times 10^{-3}$	[34]
$F_{B_d} = 190.0(1.3) \text{ MeV}$	[37]	$F_{B_d} \sqrt{\hat{B}_{B_d}} = 216(10) \text{ MeV}$	[37]
$F_{B_s} = 230.3(1.3) \text{ MeV}$	[37]	$F_{B_s} \sqrt{\hat{B}_{B_s}} = 262(10) \text{ MeV}$	[37]
$\eta_B = 0.55(1)$	[38,39]		
$\Delta M_d = 0.5065(19) \text{ ps}^{-1}$	[34]	$S_{J/\psi K_S} = 0.695(19)$	[34]
$\Delta M_s = 17.756(21) \text{ ps}^{-1}$	[34]	$S_{J/\psi \phi} = 0.054(20)$	[37]
CKM parameters			
$ V_{us} = 0.2252(5)$	[34]	$ V_{cb} = (41.0 \pm 1.4) \times 10^{-3}$	[34]
$ V_{ub} = 3.72 \times 10^{-3}$	[34]	$\gamma = 68^\circ$	[34]
$ V_{cd} = 0.22507$		$ V_{cs} = 0.97348$	
$ V_{td} = 0.00856$		$ V_{ts} = 0.04027$	

$$\begin{aligned}
 \mathcal{B}_L(B_c^+ \rightarrow B^{*+}\nu\bar{\nu}) &= 1.2 \times 10^9 |C_L - C_R|^2 = 1.0 \times 10^{-8} x_U^-, \\
 \mathcal{B}_T(B_c^+ \rightarrow B^{*+}\nu\bar{\nu}) &= 1.9 \times 10^7 |C_L + C_R|^2 \\
 &\quad + 7.4 \times 10^8 |C_L - C_R|^2 \\
 &= 1.7 \times 10^{-10} x_U^+ + 6.5 \times 10^{-9} x_U^-, \\
 \mathcal{B}(B_c^+ \rightarrow B^{*+}\nu\bar{\nu}) &= 1.9 \times 10^7 |C_L + C_R|^2 \\
 &\quad + 1.9 \times 10^9 |C_L - C_R|^2 \\
 &= 1.7 \times 10^{-10} x_U^+ + 1.7 \times 10^{-8} x_U^-. \quad (17)
 \end{aligned}$$

The largest values of $\mathcal{B}(B_c^+ \rightarrow B^+\nu\bar{\nu})$ and $\mathcal{B}(B_c^+ \rightarrow B^{*+}\nu\bar{\nu})$ correspond to the largest x_U^+ and x_U^- , respectively. We scan the branching fractions using $x_U^- = 2x_U - x_U^+$ and varying $0 \leq x_U^+ \leq 2x_U$, with $x_U \leq x_U^{\max}$ for the two cases (10) (LU bound). We extend the computation up to the cLFC bound (11), which has been established by the analysis of the charged lepton modes, to investigate the size of the enhancement in this case. In Fig. 1, we show the largest enhancement for the $d\mathcal{B}(B_c^+ \rightarrow B^+\nu\bar{\nu})/dx$ distribution obtained for $x_U^+ = 2x_U$. In Fig. 2, we depict the maximum enhancement for the missing energy distribution and for the distributions of longitudinally and transversely polarized B^{*+} in $B_c^+ \rightarrow B^{*+}\nu\bar{\nu}$. Integrating over x we have

$$\begin{aligned}
 \mathcal{B}(B_c^+ \rightarrow B^+\nu\bar{\nu})_{\text{LU}}^{\max} &= (4.7 \pm 0.25) \times 10^{-7}, \\
 \mathcal{B}(B_c^+ \rightarrow B^+\nu\bar{\nu})_{\text{cLFC}}^{\max} &= (2.7 \pm 0.15) \times 10^{-6}, \quad (18)
 \end{aligned}$$

$$\begin{aligned}
 \mathcal{B}(B_c^+ \rightarrow B^{*+}\nu\bar{\nu})_{\text{LU}}^{\max} &= (1.1 \pm 0.06) \times 10^{-6}, \\
 \mathcal{B}(B_c^+ \rightarrow B^{*+}\nu\bar{\nu})_{\text{cLFC}}^{\max} &= (6.5 \pm 0.3) \times 10^{-6}. \quad (19)
 \end{aligned}$$

The largest values of the branching fractions must be compared with the SM prediction from Eq. (3), $\mathcal{B}(B_c^+ \rightarrow B^+\nu\bar{\nu})^{\text{SM}} = (8.5 \pm 0.5) \times 10^{-18}$, $\mathcal{B}(B_c^+ \rightarrow B^{*+}\nu\bar{\nu})^{\text{SM}} = (2.1 \pm 0.1) \times 10^{-17}$, and with the estimate of the long-distance

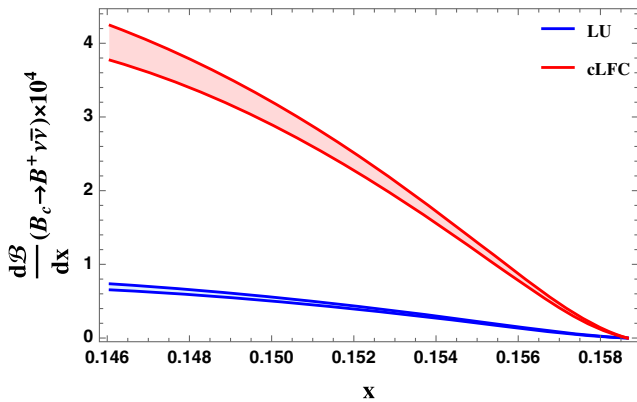


FIG. 1. Missing energy distribution $d\mathcal{B}(B_c^+ \rightarrow B^+\nu\bar{\nu})/dx$ for the largest value of the coefficients combination x_U in Eqs. (10) (LU bound, blue curve) and (11) (cLFC bound, red curve). The widths of the curves are obtained varying the form factor parameters [3,28].

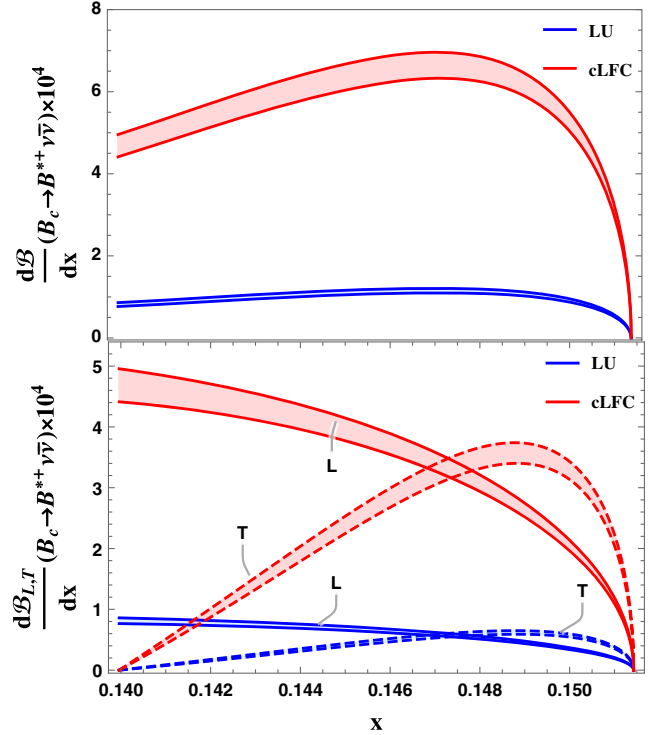


FIG. 2. Missing energy distributions $d\mathcal{B}(B_c^+ \rightarrow B^{*+}\nu\bar{\nu})/dx$ (top) and $d\mathcal{B}_{L,T}(B_c^+ \rightarrow B^{*+}\nu\bar{\nu})/dx$ (bottom) for x_U^{\max} in Eqs. (10) (blue curves) and (11) (red curves). The widths of the curves are obtained varying the form factor parameters.

contributions discussed in the Appendix. Hence, a huge enhancement with respect to tiny SM prediction is possible. Setting x_U below the bounds (10) and (11) and varying $x_U^+ \in [0, 2x_U]$, the branching fractions can be read in the plot in Fig. 3.

The enhancements in Eqs. (18) and (19), achievable in generic NP scenarios, must be taken with caution, since they would be the manifestation of BSM phenomena affecting other processes to a level that is necessary to control. For this reason, it is worth considering a well defined extension of the Standard Model, as discussed in the next section.

IV. $c \rightarrow u\ell\bar{\nu}$ TRANSITION IN THE 331 MODEL

Among the extensions of the Standard Model, we focus on the 331 models, a class of models based on the gauge group $SU(3)_C \times SU(3)_L \times U(1)_X$ [40,41]. The gauge symmetry is spontaneously broken to the SM group $SU(3)_C \times SU(2)_L \times U(1)_Y$, followed by the spontaneous breaking to $SU(3)_C \times U(1)_Q$. This extension of the gauge group has remarkable features. Left-handed fermions transform under $SU(3)_L$ either as triplets or as antitriplets. The requirement of gauge anomaly cancellation imposes that the number of triplets should be equal to the number of antitriplets. This constraint together with the asymptotic freedom of QCD imposes that the number of fermion

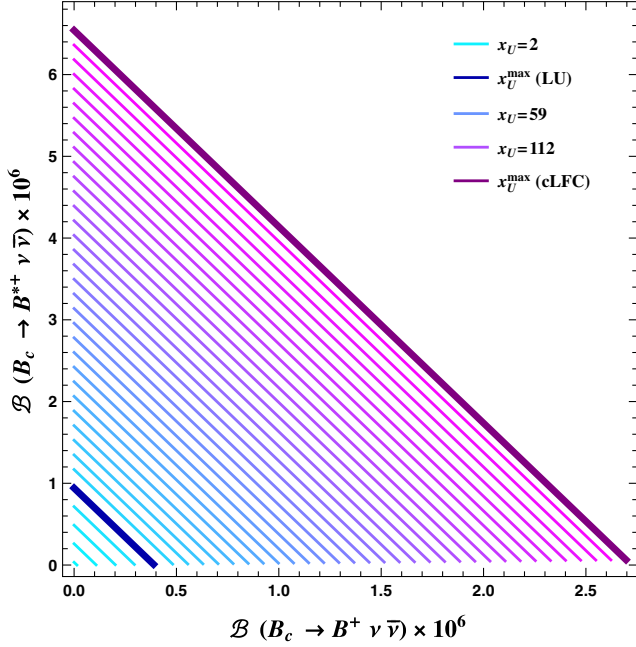


FIG. 3. Anticorrelation between $\mathcal{B}(B_c^+ \rightarrow B^{*+} \nu \bar{\nu})$ and $\mathcal{B}(B_c^+ \rightarrow B^{*+} \nu \bar{\nu}) \times 10^6$, varying the combination of the coefficients x_U up to the bounds in Eqs. (10) and (11). Colors from cyan to magenta indicate increasing values of x_U . The dark blue line corresponds to the value saturating the LU bound and the dark purple line to the value saturating the cLFC bound. The colors corresponding to three other representative values of x_U (2,59,112) are also indicated in the legend.

generations is equal to the number of colors, a hint of why there are three generations in nature. The quark generations transform differently under $SU(3)_L$, and a possibility is that two left-handed quark generations transform as $SU(3)_L$ triplets and one as an antitriplet. Choosing the latter one as the third generation, the different assignment can be a hint of why there is a large top mass.

$$V_L = \begin{pmatrix} \tilde{c}_{12}\tilde{c}_{13} & \tilde{s}_{12}\tilde{c}_{23}e^{i\delta_3} - \tilde{c}_{12}\tilde{s}_{13}\tilde{s}_{23}e^{i(\delta_1-\delta_2)} & \tilde{c}_{12}\tilde{c}_{23}\tilde{s}_{13}e^{i\delta_1} + \tilde{s}_{12}\tilde{s}_{23}e^{i(\delta_2+\delta_3)} \\ -\tilde{c}_{13}\tilde{s}_{12}e^{-i\delta_3} & \tilde{c}_{12}\tilde{c}_{23} + \tilde{s}_{12}\tilde{s}_{13}\tilde{s}_{23}e^{i(\delta_1-\delta_2-\delta_3)} & -\tilde{s}_{12}\tilde{s}_{13}\tilde{c}_{23}e^{i(\delta_1-\delta_3)} - \tilde{c}_{12}\tilde{s}_{23}e^{i\delta_2} \\ -\tilde{s}_{13}e^{-i\delta_1} & -\tilde{c}_{13}\tilde{s}_{23}e^{-i\delta_2} & \tilde{c}_{13}\tilde{c}_{23} \end{pmatrix}, \quad (22)$$

with $\tilde{c}_i = \cos \theta_i$, $\tilde{s}_i = \sin \theta_i$, and phases $\delta_{1,2,3}$. With this parametrization, considering the Z' couplings to the quarks, one finds that the B_d system involves the parameters \tilde{s}_{13} and δ_1 , the B_s system \tilde{s}_{23} and δ_2 , and the kaon system \tilde{s}_{13} , \tilde{s}_{23} , and $\delta_2 - \delta_1$. This provides remarkable correlations among observables in kaon, B_d , and B_s systems [42–46].

It is interesting to observe that the relation

$$U_L = V_L \cdot V_{\text{CKM}}^\dagger \quad (23)$$

The electric charge generator Q is defined by

$$Q = T_3 + \beta T_8 + X, \quad (20)$$

with T_3 and T_8 the diagonal $SU(3)_L$ and X the $U(1)_X$ generators. The parameter β defines the specific variant of the model. Four new gauge bosons have integer electric charges if β is a multiple of $\frac{1}{\sqrt{3}}$ and $\sqrt{3}$. The $U(1)_X$ gauge coupling g_X and the $SU(3)_L$ coupling g are related,

$$\frac{g_X^2}{g^2} = \frac{6 \sin^2 \theta_W}{1 - (1 + \beta^2) \sin^2 \theta_W}. \quad (21)$$

Equation (21) provides the bound $|\beta| \leq \frac{1}{\tan \theta_W(M_{Z'})}$ which corresponds to $|\beta| < 1.737$ for the sine of the Weinberg angle $\sin \theta_W(M_{Z'} = 1 \text{ TeV}) = 0.249$.

In all the 331 variants, there is a neutral gauge boson Z' mediating tree-level FCNC in the quark sector, with universal and diagonal Z' couplings to leptons. The extended Higgs sector involves three $SU(3)_L$ triplets and one sextet. New heavy fermions are also present in the spectrum.

As in the SM, quark mass eigenstates are defined upon rotation of flavor eigenstates through two unitary matrices, U_L (for up-type quarks) and V_L (for down-type quarks). The relation $V_{\text{CKM}} = U_L^\dagger V_L$ holds. However, while in the SM, V_{CKM} only enters in charged current interactions, and the two rotation matrices do not appear individually. In 331 model, only one matrix, either U_L or V_L , can be expressed in terms of V_{CKM} and of the other one. The remaining rotation matrix affects the Z' couplings to the quarks. Choosing V_L as the surviving rotation matrix, it can be parametrized as

allows us to bound the Z' mediated FCNC transitions of up-type quarks using the constraints established in the down-type quark sector [47]. Such a relation connecting the down-type and up-type quark FCNC processes is a peculiar feature of the 331 model.

The Z' coupling to ordinary fermions, for a generic value of the β parameter, is encoded in the 331 Lagrangian density,

$$\begin{aligned}
 iL_{\text{int}}^{Z'} &= i \frac{gZ'^\mu}{2\sqrt{3}c_W\sqrt{1-(1+\beta^2)s_W^2}} \\
 &\times \left\{ \sum_{\ell=e,\mu,\tau} \{ [1 - (1 + \sqrt{3}\beta)s_W^2] (\bar{\nu}_{\ell L}\gamma_\mu\nu_{\ell L} + \bar{\ell}_L\gamma_\mu\ell_L) - 2\sqrt{3}\beta s_W^2 \bar{\ell}_R\gamma_\mu\ell_R \} \right. \\
 &+ \sum_{i,j=1,2,3} \left\{ \left[-1 + \left(1 + \frac{\beta}{\sqrt{3}} \right) s_W^2 \right] (\bar{q}_{uL})_i \gamma_\mu (q_{uL})_j \delta_{ij} + 2c_W^2 (\bar{q}_{uL})_i \gamma_\mu (q_{uL})_j u_{3i}^* u_{3j} \right. \\
 &+ \left[-1 + \left(1 + \frac{\beta}{\sqrt{3}} \right) s_W^2 \right] (\bar{q}_{dL})_i \gamma_\mu (q_{dL})_j \delta_{ij} + 2c_W^2 (\bar{q}_{dL})_i \gamma_\mu (q_{dL})_j v_{3i}^* v_{3j} \\
 &\left. \left. + \frac{4}{\sqrt{3}} \beta s_W^2 (\bar{q}_{uR})_i \gamma_\mu (q_{uR})_j \delta_{ij} - \frac{2}{\sqrt{3}} \beta s_W^2 (\bar{q}_{dR})_i \gamma_\mu (q_{dR})_j \delta_{ij} \right\} \right, \tag{24}
 \end{aligned}$$

where $s_W = \sin\theta_W$, $c_W = \cos\theta_W$, $q_u(q_d)$ denotes an up (down)-type quark (i, j are generation indices), and v_{ij} and u_{ij} are the elements of the V_L and U_L matrices, respectively. The models corresponding to $\beta = \pm \frac{2}{\sqrt{3}}$ and $\beta = \pm \frac{1}{\sqrt{3}}$, together with the choice of the fermions in the third generation as transforming as $SU(3)_L$ antitriplets, satisfy a number of phenomenological constraints [43]. In particular, it is possible to select a region of the parameter space compatible with the constraints from $\Delta F = 2$ observables in the B_d , B_s , and K systems and from the electroweak precision observables, provided that the Z' mass is not lighter than 1 TeV. In the variant with $\beta = \frac{2}{\sqrt{3}}$, relevant contributions are predicted to the ratio $\frac{\xi}{\epsilon}$ [45].

As shown in [44], the $Z - Z'$ mixing can be neglected in $\Delta F = 2$ transitions, while it must be taken into account in decays with neutrinos in the final state. The $Z - Z'$ mixing angle is written as [44]

$$\begin{aligned}
 \sin\xi &= \frac{c_W^2}{3} \sqrt{f(\beta)} \left(3\beta \frac{s_W^2}{c_W^2} + \sqrt{3}a \right) \frac{M_Z^2}{M_{Z'}^2} \\
 &= B(\beta, a) \frac{M_Z^2}{M_{Z'}^2}, \tag{25}
 \end{aligned}$$

where

$$f(\beta) = \frac{1}{1 - (1 + \beta^2)s_W^2} > 0 \tag{26}$$

and

$$-1 < a = \frac{v_-^2}{v_+^2} < 1. \tag{27}$$

v_\pm^2 are given in terms of the vacuum expectation values of two Higgs triplets ρ and η ,

$$v_+^2 = v_\eta^2 + v_\rho^2, \quad v_-^2 = v_\eta^2 - v_\rho^2. \tag{28}$$

The parameter a is expressed in terms of $\tan\bar{\beta} = \frac{v_\rho}{v_\eta}$ as in two Higgs doublet models [we use $\bar{\beta}$ to distinguish this parameter from β defining the 331 model in (20)] [44],

$$a = \frac{1 - \tan^2\bar{\beta}}{1 + \tan^2\bar{\beta}}. \tag{29}$$

We consider the four variants scrutinized in [43]. For the modes with a neutrino-antineutrino pair in the final state, the $Z - Z'$ mixing is included replacing

$$\Delta_L^{\nu\bar{\nu}}(Z') \rightarrow \Delta_L^{\nu\bar{\nu}}(Z')(1 + R_{\nu\bar{\nu}}^L(a)). \tag{30}$$

$R_{\nu\bar{\nu}}^L(a)$ is defined as

$$R_{\nu\bar{\nu}}^L(a) = B(\beta, a) \frac{\Delta_{\nu\bar{\nu}}(Z)}{\Delta_L^{\nu\bar{\nu}}(Z')}, \tag{31}$$

with $B(\beta, a)$ in (25) and $\Delta_{\nu\bar{\nu}}(Z)$ the SM Z coupling to neutrinos.

In the 331 model, the $B_c \rightarrow B^{(*)+}\nu\bar{\nu}$ modes present several features. The structure of the 331 model allows us to use data from B and K decays to constrain $c \rightarrow u$ modes. Moreover, Z' mediates FCNC at tree level only in the case of left-handed quarks; hence, the coefficient C_R in the Hamiltonian (1) vanishes in all the model variants.

Considering the contribution from the tree-level diagram in Fig. 4 and using the coupling of Z' to quarks and neutrinos derived from Eq. (24), the coefficient C_L in (1)

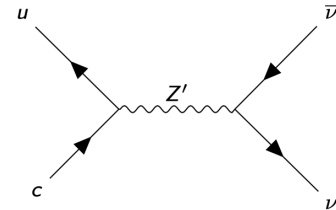


FIG. 4. Tree-level Z' contribution to the $c \rightarrow u\nu\bar{\nu}$ effective Hamiltonian.

reads

$$C_L^{331} = \frac{\Delta_L^{uc}(Z')\Delta_L^{\nu\bar{\nu}}(Z')}{M_{Z'}^2}(1 + R_{\nu\bar{\nu}}^L(a)), \quad (32)$$

where

$$\begin{aligned} \Delta_L^{uc}(Z') &= \frac{g c_W}{\sqrt{3}\sqrt{1 - (1 + \beta^2)s_W^2}} u_{31}^* u_{32}, \\ \Delta_L^{\nu\bar{\nu}}(Z') &= \frac{g[1 - (1 + \sqrt{3}\beta)s_W^2]}{2\sqrt{3}c_W\sqrt{1 - (1 + \beta^2)s_W^2}}. \end{aligned} \quad (33)$$

The elements u_{ij} are obtained from Eqs. (22) and (23). As a consequence, C_L depends on the parameters \tilde{s}_{13} , δ_1 , \tilde{s}_{23} , δ_2 that in pair control the B_d and B_s decays, respectively, and altogether govern the K decays. C_L also depends on the $Z - Z'$ mixing parameter a . The $B_c^+ \rightarrow B^{(*)+}\nu\bar{\nu}$ processes must be studied in such a parameter space.

V. $B_c^+ \rightarrow B^{(*)+}\nu\bar{\nu}$ DECAYS IN THE 331 MODEL

In the numerical analysis of $B_c^+ \rightarrow B^{(*)+}\nu\bar{\nu}$ in the 331 model, we follow the method described in [45]. We select the model parameters imposing that ΔM_{B_d} , $S_{J/\psi K_S}$, and ΔM_{B_s} , $S_{J/\psi\phi}$, whose measurements are quoted in Table I, lie in their experimental ranges within 2σ . In the kaon sector, we require that ε_K is in the range $[1.6, 2.5] \times 10^{-3}$, and ΔM_K varies between $[0.75, 1.25] \times (\Delta M_K)_{\text{SM}}$, i.e., $(\Delta M_K)_{\text{SM}} = 0.0047$ GeV using V_{ub} in Table I. The formulas for such observables in the SM and in 331 models can be found in [42]. For ε_K , we use the updated result in [48]. The other input quantities are also collected in Table I. For the CKM matrix elements, the Table displays the four entries chosen as the independent ones, the others are derived.

The obtained allowed regions in the parameter space \tilde{s}_{13} , δ_1 , \tilde{s}_{23} , δ_2 are in Fig. 5 for $M_{Z'} \in [1, 5]$ TeV. The regions $(\tilde{s}_{13}, \delta_1)$ are obtained imposing the constraints on ΔM_{B_d} , $S_{J/\psi K_S}$, the regions $(\tilde{s}_{23}, \delta_2)$ using ΔM_{B_s} , $S_{J/\psi\phi}$. In our

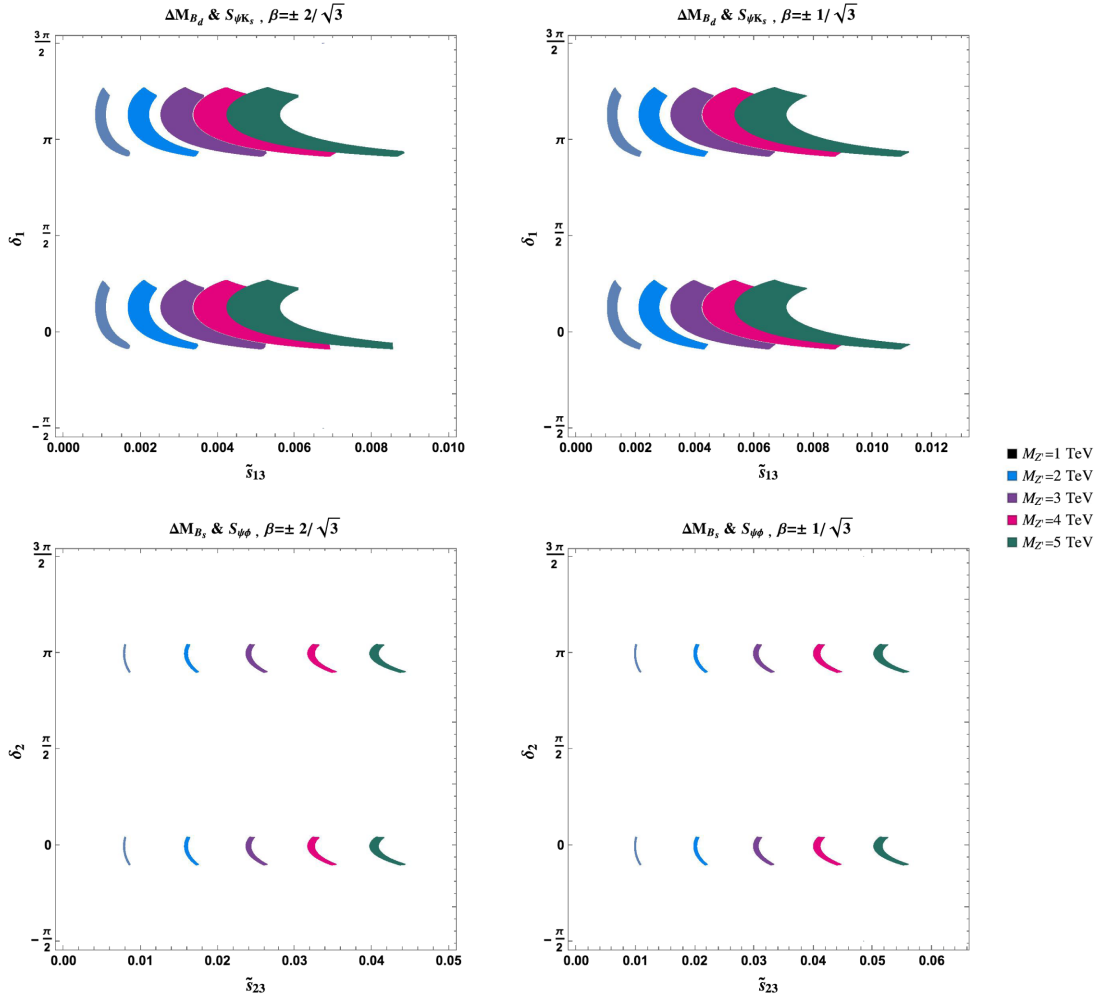


FIG. 5. Allowed regions in the 331 space of parameters \tilde{s}_{13} , δ_1 (top) and \tilde{s}_{23} , δ_2 (bottom) for $\beta = \pm \frac{2}{\sqrt{3}}$ (left) and $\beta = \pm \frac{1}{\sqrt{3}}$ (right), varying the Z' mass in the range $[1, 5]$ TeV.

computation of the observables in the 331 model, we vary $\tilde{s}_{13}, \delta_1, \tilde{s}_{23}, \delta_2$ in their allowed ranges and select the values for which the constraints from $\Delta F = 2$ processes in the kaon sector are also satisfied. For each value of β , Fig. 5 shows the presence of two ranges for the phases $\delta_{1,2}$ which are independent of $M_{Z'}$. Choosing the 331 parameters in the allowed ranges, the coefficient C_L^{331} can be computed, and the $B_c \rightarrow B^{(*)+}\nu\bar{\nu}$ branching fractions can be predicted.

In Fig. 6, we plot the missing energy distributions for the set of $\tilde{s}_{13}, \delta_1, \tilde{s}_{23}, \delta_2$, and a maximizing the dineutrino B_c branching fractions for each $M_{Z'}$ up to 5 TeV. In all cases, the choice $a = 1$ provides the largest enhancement. The central values of the branching fractions are

$$\begin{aligned} \mathcal{B}(B_c^+ \rightarrow B^+\nu\bar{\nu}) &= \frac{4.91}{(M_{Z'}/\text{GeV})^4}, & \left(\beta = -\frac{2}{\sqrt{3}}\right), \\ \mathcal{B}(B_c^+ \rightarrow B^+\nu\bar{\nu}) &= \frac{4.31}{(M_{Z'}/\text{GeV})^4}, & \left(\beta = +\frac{2}{\sqrt{3}}\right), \\ \mathcal{B}(B_c^+ \rightarrow B^+\nu\bar{\nu}) &= \frac{2.60}{(M_{Z'}/\text{GeV})^4}, & \left(\beta = -\frac{1}{\sqrt{3}}\right), \\ \mathcal{B}(B_c^+ \rightarrow B^+\nu\bar{\nu}) &= \frac{2.48}{(M_{Z'}/\text{GeV})^4}, & \left(\beta = +\frac{1}{\sqrt{3}}\right), \end{aligned} \quad (34)$$

and

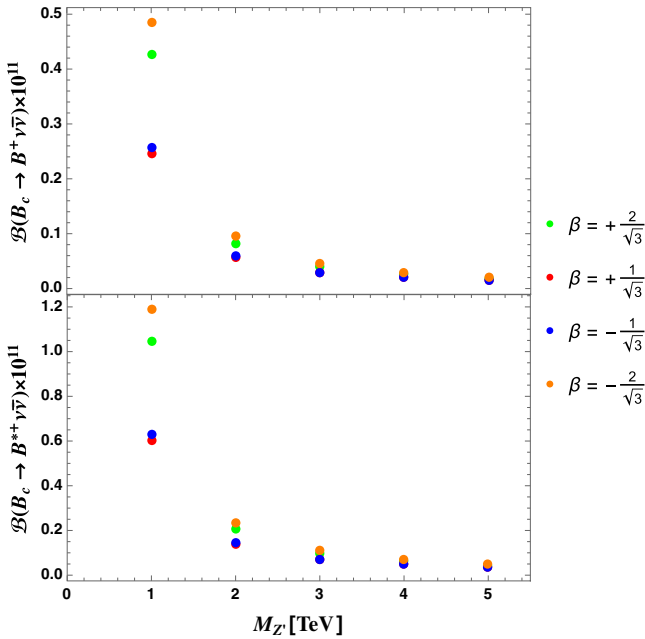


FIG. 6. Branching ratios $\mathcal{B}(B_c^+ \rightarrow B^+\nu\bar{\nu})$ and $\mathcal{B}(B_c^+ \rightarrow B^{*+}\nu\bar{\nu})$ in 331 model for $\beta = \pm\frac{2}{\sqrt{3}}$ and $\beta = \pm\frac{1}{\sqrt{3}}$, varying $M_{Z'}$ from 1 to 5 TeV. The results correspond to the values of $\tilde{s}_{13}, \delta_1, \tilde{s}_{23}, \delta_2$, and a producing the largest rates.

$$\begin{aligned} \mathcal{B}(B_c^+ \rightarrow B^{*+}\nu\bar{\nu}) &= \frac{12.02}{(M_{Z'}/\text{GeV})^4}, & \left(\beta = -\frac{2}{\sqrt{3}}\right), \\ \mathcal{B}(B_c^+ \rightarrow B^{*+}\nu\bar{\nu}) &= \frac{10.56}{(M_{Z'}/\text{GeV})^4}, & \left(\beta = +\frac{2}{\sqrt{3}}\right), \\ \mathcal{B}(B_c^+ \rightarrow B^{*+}\nu\bar{\nu}) &= \frac{6.36}{(M_{Z'}/\text{GeV})^4}, & \left(\beta = -\frac{1}{\sqrt{3}}\right), \\ \mathcal{B}(B_c^+ \rightarrow B^{*+}\nu\bar{\nu}) &= \frac{6.08}{(M_{Z'}/\text{GeV})^4}, & \left(\beta = +\frac{1}{\sqrt{3}}\right). \end{aligned} \quad (35)$$

The enhancement with respect to the SM is large, even though the branching fractions do not exceed $\mathcal{O}(10^{-11})$.

VI. CORRELATIONS BETWEEN THE MODES $c \rightarrow u\nu\bar{\nu}$ AND $s \rightarrow d\nu\bar{\nu}, b \rightarrow s\nu\bar{\nu}$ IN THE 331 MODEL

We have remarked that a peculiar feature of the 331 model is the possibility of constraining FCNC up-type quark processes using information on FCNC down-type quark transitions. On this basis, we can establish the correlations between $B_c \rightarrow B^{(*)+}\nu\bar{\nu}$ and the $s \rightarrow d\nu\bar{\nu}$ induced transitions $K^+ \rightarrow \pi^+\nu\bar{\nu}$ and $K_L \rightarrow \pi^0\nu\bar{\nu}$ and between $B_c \rightarrow B^{(*)+}\nu\bar{\nu}$ and $B \rightarrow \{X_s, K, K^*\}\nu\bar{\nu}$ induced by $b \rightarrow s\nu\bar{\nu}$. In the SM, such transitions proceed through box and Z^0 penguin diagrams. The low-energy $s \rightarrow d\nu\bar{\nu}$ Hamiltonian reads in the SM as

$$\begin{aligned} H_{\text{eff}}^{\bar{s} \rightarrow d\nu\bar{\nu}}|_{\text{SM}} &= 4 \frac{G_F}{\sqrt{2}} \frac{\alpha}{2\pi \sin^2 \theta_W} \\ &\times \sum_{\ell=e,\mu,\tau} [V_{cs}^* V_{cd} X_{\text{NNL}}^\ell(x_c) + V_{ts}^* V_{td} X(x_t)] \\ &\times (\bar{s}\gamma_\mu P_L d)(\bar{\nu}_\ell \gamma_\mu P_L \nu_\ell) + \text{H.c.}, \end{aligned} \quad (36)$$

with $x_i = m_i^2/M_W^2$. $X_{\text{NNL}}^\ell(x_c)$ takes into account the internal charm contribution [49–54]; the function

$$X(x_t) = \eta_X \frac{x_t}{8} \left[\frac{x_t + 2}{x_t - 1} + \frac{3x_t - 6}{(x_t - 1)^2} \ln x_t \right] \quad (37)$$

describes the internal top contribution. $\eta_X = 0.994$ is a QCD correction computed for $m_t = m_t(m_t)$ [50,55]. In the charged $K^+ \rightarrow \pi^+\nu\bar{\nu}$ mode, both contributions must be taken into account; in $K_L \rightarrow \pi^0\nu\bar{\nu}$, the top quark contribution dominates. The top quark contribution also dominates in the $b \rightarrow s\nu\bar{\nu}$ modes governed by the effective Hamiltonian

$$\begin{aligned} H_{\text{eff}}^{b \rightarrow s\nu\bar{\nu}}|_{\text{SM}} &= 4 \frac{G_F}{\sqrt{2}} \frac{\alpha}{2\pi \sin^2 \theta_W} \\ &\times \sum_{\ell=e,\mu,\tau} [V_{ts}^* V_{tb} X(x_t)] (\bar{s}\gamma^\mu P_L b)(\bar{\nu}_\ell \gamma_\mu P_L \nu_\ell) \\ &+ \text{H.c.} \end{aligned} \quad (38)$$

The 331 contribution from the tree-level Z' exchange can be included in the Hamiltonian replacing $X(x_i) \rightarrow X(M)$ with

$$X(M) = X(x_i) + \Delta X^i(M) \quad (39)$$

and

$$\left[4 \frac{G_F}{\sqrt{2}} \frac{\alpha}{2\pi \sin^2 \theta_W} V_{ts}^* V_{td} \right] \Delta X^{sd}(K) = \frac{\Delta_L^{sd}(Z') \Delta_L^{\nu\bar{\nu}}(Z')}{M_{Z'}^2}, \quad (40)$$

$$\left[4 \frac{G_F}{\sqrt{2}} \frac{\alpha}{2\pi \sin^2 \theta_W} V_{ts}^* V_{tb} \right] \Delta X^{bs}(B) = \frac{\Delta_L^{bs}(Z') \Delta_L^{\nu\bar{\nu}}(Z')}{M_{Z'}^2}. \quad (41)$$

The $Z - Z'$ mixing is included multiplying the rhs of Eqs. (40) and (41) by $(1 + R_{\nu\bar{\nu}}^L(a))$, with $R_{\nu\bar{\nu}}^L$ in (31).

A. Correlations with dineutrino kaon modes

In the SM, the decays $K^+ \rightarrow \pi^+ \nu \bar{\nu}$ and $K_L \rightarrow \pi^0 \nu \bar{\nu}$ are predicted with branching ratios of $\mathcal{O}(10^{-11})$. The processes are theoretically well controlled, due to the possibility of relating their hadronic matrix elements to the precisely measured semileptonic $K^+ \rightarrow \pi^0 e^+ \nu_e$ matrix element. The NA62 Collaboration at CERN has measured $\mathcal{B}(K^+ \rightarrow \pi^+ \nu \bar{\nu}) = (10.6 \pm_{3.4}^{4.0} |_{\text{stat}} \pm 0.9_{\text{syst}}) \times 10^{-11}$ at 68% C.L. [5]. The upper bound for the neutral mode is $\mathcal{B}(K_L \rightarrow \pi^0 \nu \bar{\nu}) < 3.9 \times 10^{-9}$ (at 90% C.L.) [6,7]. Detailed discussions of the dineutrino kaon modes in the SM and in the 331 model are presented in Refs. [4] and [42–46]. The branching ratios are expressed in the form

$$\mathcal{B}(K^+ \rightarrow \pi^+ \nu \bar{\nu}) = \kappa_+ (1 + \Delta_{\text{EM}}) \left[\left(\frac{\text{Im} X_{\text{eff}}}{\lambda^5} \right)^2 + \left(\frac{\text{Re} X_{\text{eff}}}{\lambda^5} - P_c(X) \right)^2 \right], \quad (42)$$

$$\mathcal{B}(K_L \rightarrow \pi^0 \nu \bar{\nu}) = \kappa_L \left(\frac{\text{Im} X_{\text{eff}}}{\lambda^5} \right)^2, \quad (43)$$

with $\lambda = |V_{us}|$ in Table I. The other quantities are

$$\begin{aligned} \kappa_+ &= (5.21 \pm 0.025) \left[\frac{\lambda}{0.2252} \right]^8 \times 10^{-11}, \\ \kappa_L &= (2.247 \pm 0.013) \left[\frac{\lambda}{0.2252} \right]^8 \times 10^{-10}, \\ P_c(X) &= 0.405 \pm 0.024, \\ \Delta_{\text{EM}} &= -0.03, \\ X_{\text{eff}} &= V_{ts}^* V_{td} X(K), \end{aligned} \quad (44)$$

with $X(K)$ in Eqs. (39) and (40) [51–53,56,57].

In Figs. 7 and 8, we show the correlations between $\mathcal{B}(B_c \rightarrow B^{(*)+} \nu \bar{\nu})$ and $\mathcal{B}(K^+ \rightarrow \pi^+ \nu \bar{\nu})$ and in Figs. 9 and 10 the correlations with $\mathcal{B}(K_L \rightarrow \pi^0 \nu \bar{\nu})$. The Z' mass is set to $M_{Z'} = 1$ TeV, and the results for heavier Z' can be obtained by a simple rescaling. For each $\beta = \pm 1/\sqrt{3}$, $\pm 2/\sqrt{3}$, the parameters \tilde{s}_{13} , δ_1 , \tilde{s}_{23} , δ_2 are varied in their allowed regions in Fig. 5. In each plot, the sliding colors represent nine values of the $Z - Z'$ mixing parameter a in the range $[-1, 1]$ (the colors corresponding to $a = -1, 0, 1$ are indicated in the legends). Only for $a = -1$ are the results compatible with the SM. For $a = 1$, the branching fractions sizably deviate from the SM prediction, and the largest enhancement of the B_c modes corresponds to a suppression of the kaon modes with respect to the SM.

B. Correlations with dineutrino B decays

Let us consider the modes $B \rightarrow M_s \nu \bar{\nu}$ ($M_s = X_s, K, K^*$). The NP effects in scenarios with a Z' with tree-level flavor-changing couplings only to left-handed fermions can be expressed in the form [10,42]

$$\mathcal{B}(B \rightarrow M_s \nu \bar{\nu}) = \mathcal{B}(B \rightarrow M_s \nu \bar{\nu})_{\text{SM}} \times q^2, \quad (45)$$

with

$$q = \frac{|X(B_s)|}{X(x_i)} \quad (46)$$

and $X(B_s)$ in Eqs. (39) and (41). The SM terms are [4,10,12]

$$\mathcal{B}(B \rightarrow X_s \nu \bar{\nu})_{\text{SM}} = (3.0 \pm 0.3) \times 10^{-5}, \quad (47)$$

$$\mathcal{B}(B^+ \rightarrow K^+ \nu \bar{\nu})_{\text{SM}} = (4.35 \pm 0.59) \times 10^{-6}, \quad (48)$$

$$\mathcal{B}(B^0 \rightarrow K^{*0} \nu \bar{\nu})_{\text{SM}} = (9.44 \pm 0.89) \times 10^{-6}. \quad (49)$$

They can be compared to the experimental upper bounds (at 90% C.L.) [20,22],

$$\mathcal{B}(B^+ \rightarrow K^+ \nu \bar{\nu})_{\text{exp}} \leq 1.6 \times 10^{-5}, \quad (50)$$

$$\mathcal{B}(B \rightarrow K^* \nu \bar{\nu})_{\text{exp}} \leq 2.7 \times 10^{-5}. \quad (51)$$

The correlations between $\mathcal{B}(B_c \rightarrow B^+ \nu \bar{\nu})$ and $\mathcal{B}(B \rightarrow (X_s, K, K^*) \nu \bar{\nu})$ for $\beta = -\frac{2}{\sqrt{3}}, -\frac{1}{\sqrt{3}}$ are in Figs. 11 and 12. The correlations for the vector $B_c \rightarrow B^{*+} \nu \bar{\nu}$ mode have the same pattern, differing only for the $\mathcal{B}(B_c \rightarrow B^{*+} \nu \bar{\nu})$ scale factor. The sliding colors describe the variation of $a \in [-1, 1]$; the 331 result is compatible with the SM for $a = -1$. The largest enhancements of $\mathcal{B}(B_c \rightarrow B^+ \nu \bar{\nu})$ correspond to a suppression of $b \rightarrow s \nu \bar{\nu}$ with respect to the SM.

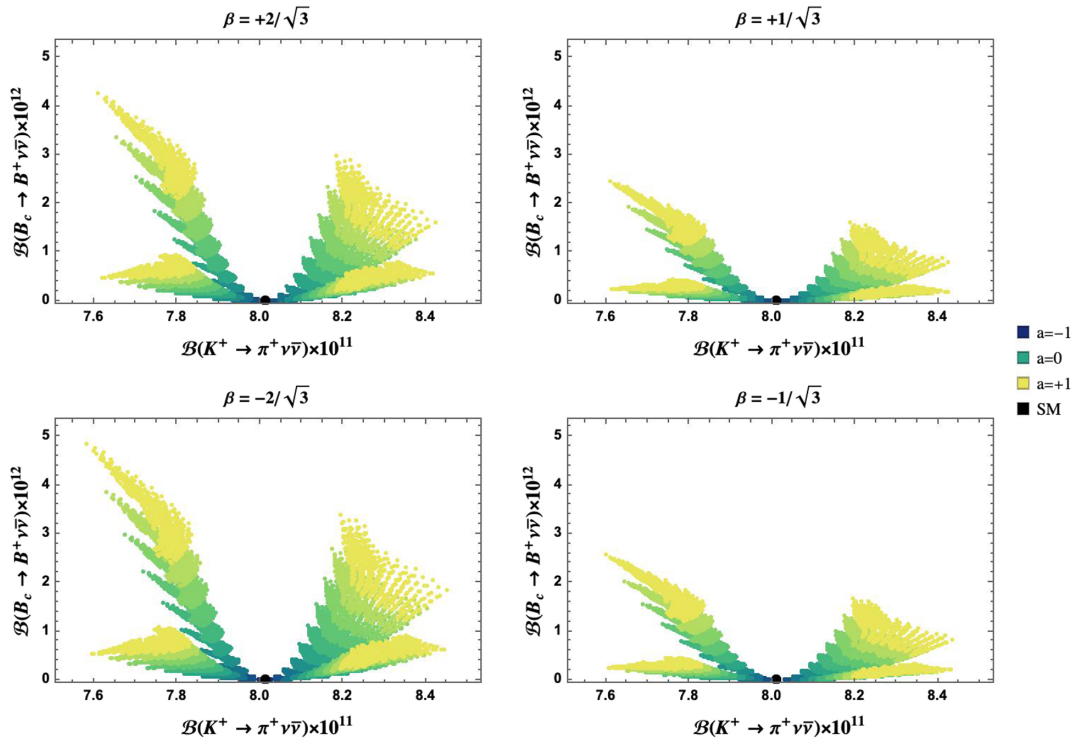


FIG. 7. Correlations between the branching fractions $\mathcal{B}(B_c \rightarrow B^+\nu\bar{\nu})$ and $\mathcal{B}(K^+ \rightarrow \pi^+\nu\bar{\nu})$ in the 331 model with $\beta = \frac{2}{\sqrt{3}}, \frac{1}{\sqrt{3}}, -\frac{2}{\sqrt{3}}, -\frac{1}{\sqrt{3}}$, $M_{Z'} = 1$ TeV and $Z - Z'$ mixing parameter $a = -1, 0, 1$. The black dot is the SM result.

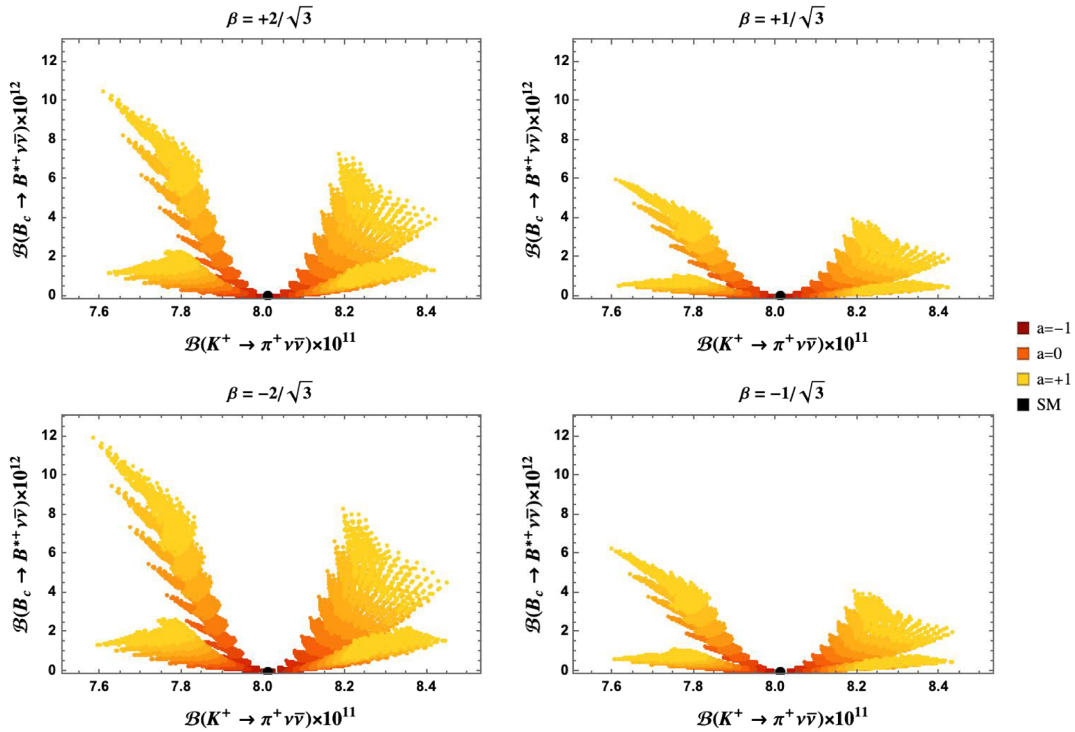


FIG. 8. Correlations between $\mathcal{B}(B_c \rightarrow B^{*+}\nu\bar{\nu})$ and $\mathcal{B}(K^+ \rightarrow \pi^+\nu\bar{\nu})$ in the 331 model with parameters as in Fig. 7. The black dot is the SM result.

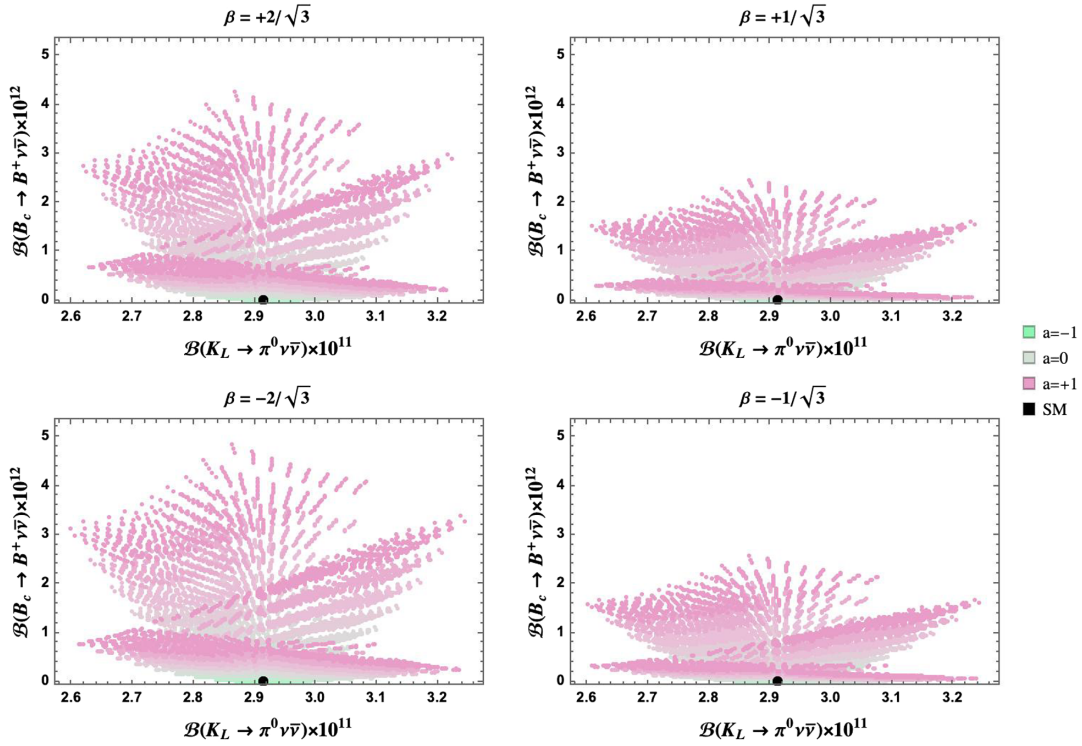


FIG. 9. Correlations between $\mathcal{B}(B_c \rightarrow B^+ \nu \bar{\nu})$ and $\mathcal{B}(K_L \rightarrow \pi^0 \nu \bar{\nu})$ in the 331 model with parameters as in Fig. 7. The black dot is the SM result.

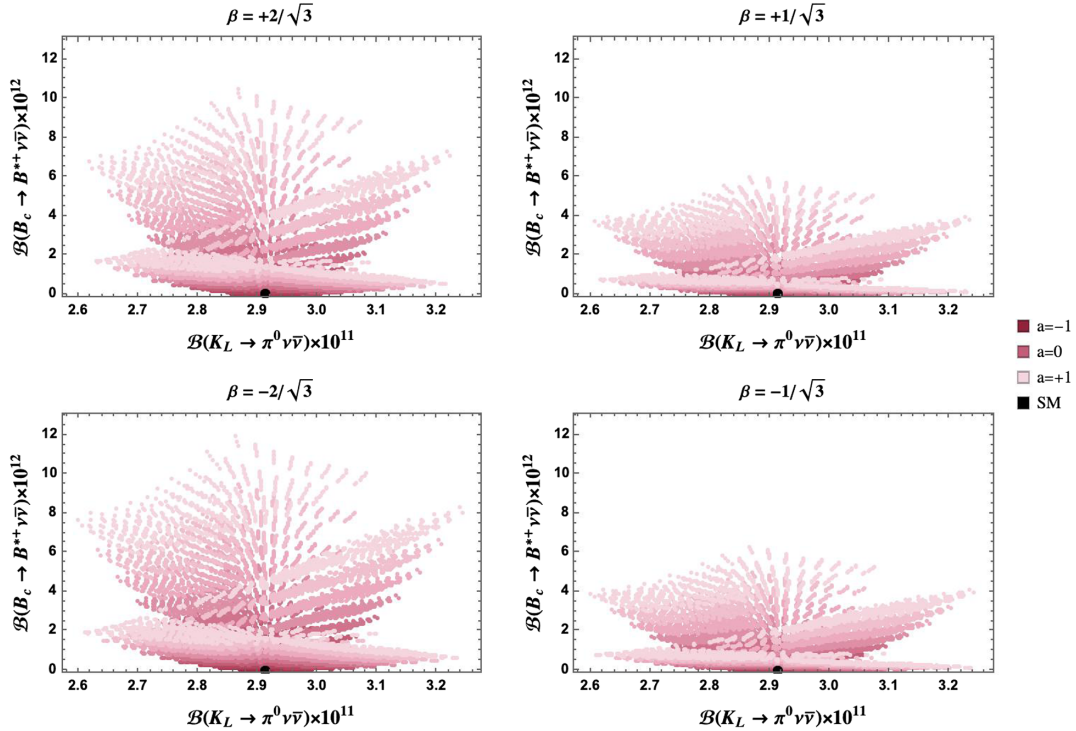


FIG. 10. Correlations between $\mathcal{B}(B_c \rightarrow B^{*+} \nu \bar{\nu})$ and $\mathcal{B}(K_L \rightarrow \pi^0 \nu \bar{\nu})$ in the 331 model with parameters as in Fig. 7. The black dot is the SM result.

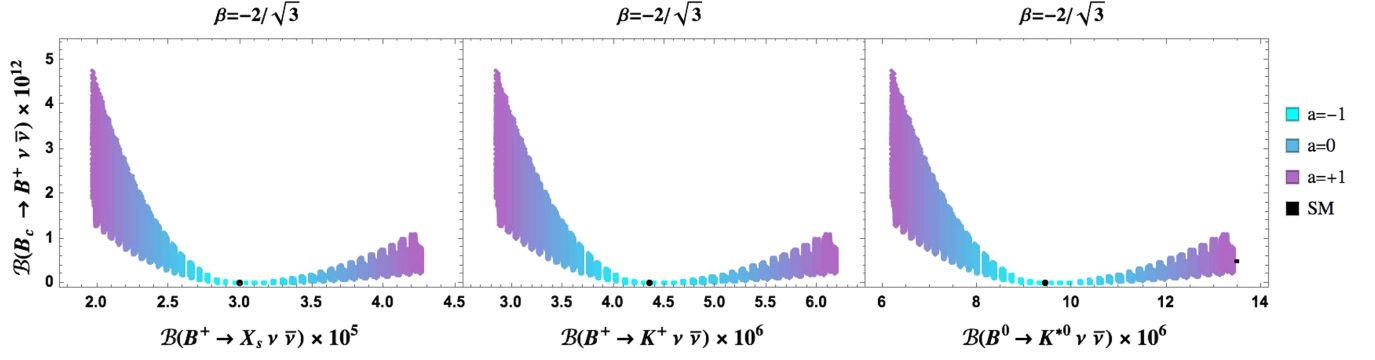


FIG. 11. Correlations between $\mathcal{B}(B_c \rightarrow B^+\nu\bar{\nu})$ and $\mathcal{B}(B^+ \rightarrow X_s\nu\bar{\nu})$ (left), $\mathcal{B}(B^+ \rightarrow K^+\nu\bar{\nu})$ (middle), and $\mathcal{B}(B^0 \rightarrow K^{*0}\nu\bar{\nu})$ (right) for $\beta = -\frac{2}{\sqrt{3}}$, $M_{Z'} = 1$ TeV. The black dot indicates the SM result.

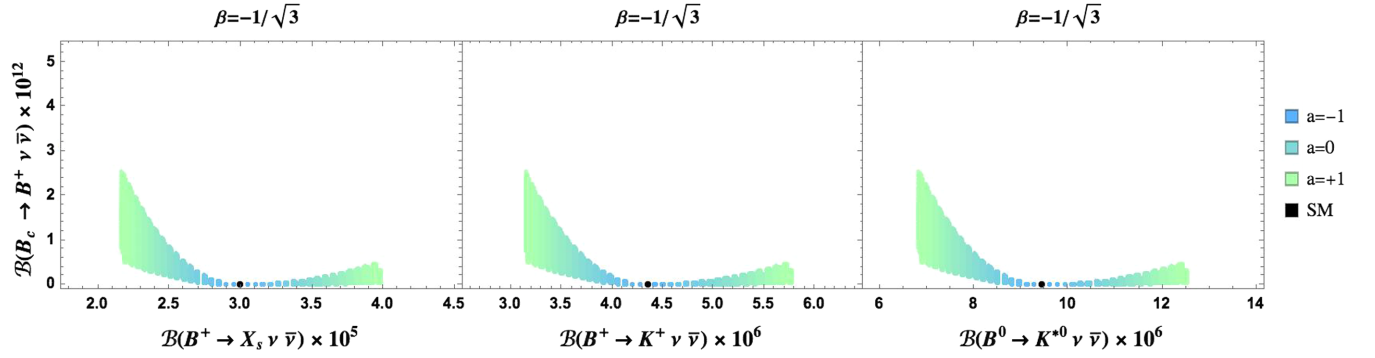


FIG. 12. Correlations between $\mathcal{B}(B_c \rightarrow B^+\nu\bar{\nu})$ and $\mathcal{B}(B^+ \rightarrow X_s\nu\bar{\nu})$ (left), $\mathcal{B}(B^+ \rightarrow K^+\nu\bar{\nu})$ (middle), and $\mathcal{B}(B^0 \rightarrow K^{*0}\nu\bar{\nu})$ (right), for $\beta = -\frac{1}{\sqrt{3}}$, $M_{Z'} = 1$ TeV. The black dot indicates the SM result.

VII. CONCLUSIONS

Null tests, like rare FCNC charm decays, are useful to investigate the existence of phenomena beyond the Standard Model. The $B_c \rightarrow B^{(*)+}\nu\bar{\nu}$ modes are predicted within the SM with branching ratios not exceeding $\mathcal{O}(10^{-16})$ and can be used for null tests. Exploiting the relations between the Wilson coefficients of $c \rightarrow u\nu\bar{\nu}$ and the $c \rightarrow u\ell^+\ell^-$ low-energy Hamiltonian obtained from the SMEFT, together with the experimental bounds on the charged dilepton $c \rightarrow u$ processes, we have derived the largest enhancement for the dineutrino modes in generic NP scenarios, finding branching fractions up to $\mathcal{O}(10^{-6})$. Specific NP scenarios predict smaller effects. To investigate this point, we have predicted the branching fractions for these processes in the 331 model. The reason to consider this framework is that in this model the NP parameters entering in FCNC charm decays are the same that govern the B, B_s, K FCNC transitions. This provides nontrivial correlations among the observables in the various systems. In the 331 models, the effective $c \rightarrow u\nu\bar{\nu}$ Hamiltonian comprises only one operator, as in the SM, with a modification of the Wilson coefficient enhancing $\mathcal{B}(B_c \rightarrow B^{(*)+}\nu\bar{\nu})$ up to $\mathcal{O}(10^{-11})$. Moreover, in this model, a correlation with down-type quark dineutrino processes can be established. We have found that the largest branching

fractions correspond to $\beta = -2/\sqrt{3}$ and are anticorrelated with $K^+ \rightarrow \pi^+\nu\bar{\nu}$, $K_L \rightarrow \pi^0\nu\bar{\nu}$, and $B \rightarrow \{X_s, K, K^*\}\nu\bar{\nu}$.

ACKNOWLEDGMENTS

We thank A. J. Buras for enlightening discussions. This study has been carried out within the INFN project (Iniziativa Specifica) QFT-HEP.

APPENDIX: LONG-DISTANCE CONTRIBUTIONS TO $B_c \rightarrow B^{(*)+}\nu\bar{\nu}$

We estimate the main long-distance contributions to $B_c \rightarrow B^{(*)+}\nu\bar{\nu}$ represented by the processes $B_c \rightarrow B^{(*)+}V^0 \rightarrow B^{(*)+}\nu\bar{\nu}$, with $V^0 = \rho^0, \omega, \phi$ [2]. The nonleptonic color suppressed $B_c \rightarrow B^{(*)+}V^0$ amplitude can be estimated using naive factorization in terms of the $B_c \rightarrow B^{(*)}$ form factors. The $V^0 \rightarrow \nu\ell\bar{\nu}\ell$ amplitude involves the hadronic matrix elements

$$\langle 0|\bar{q}\gamma^\mu(g_V^q - g_A^q\gamma_5)q|V^0(q, \epsilon)\rangle, \quad (A1)$$

with $g_{V,A}^q$ the vector and axial-vector couplings constants of the neutral current for quarks. Actually, (A1) takes

contributions only from the vector quark current. These matrix elements can be obtained from the V^0 matrix element of the electromagnetic (em) current $J_{em}^\mu = \sum_q e_q \bar{q} \gamma^\mu q$, with e_q the quark charges, parametrized as

$$\langle 0 | J_{em}^\mu | V^0(q, \epsilon) \rangle = \frac{m_{V^0}^2}{f_{V^0}} \epsilon^\mu. \quad (\text{A2})$$

Using the V^0 masses, widths, and $V^0 \rightarrow e^+ e^- (\mu^+ \mu^-)$ branching fractions [34], we have $f_{\rho^0} = 4.99 \pm 0.03$ (5.08 ± 0.16), $f_\omega = 16.50 \pm 0.25$ (16.49 ± 2.01), and $f_\phi = 13.51 \pm 0.22$ (13.78 ± 0.51). The results for the LD contribution, $\mathcal{B}(B_c \rightarrow B^+ \nu \bar{\nu})|_{\text{LD}} \simeq 1.0 \times 10^{-16}$ and $\mathcal{B}(B_c \rightarrow B^{*+} \nu \bar{\nu})|_{\text{LD}} \simeq 9.8 \times 10^{-17}$ confirm the role of $B_c \rightarrow B^{(*)} \nu \bar{\nu}$ as null tests of the SM.

-
- [1] H. Gisbert, M. Golz, and D. S. Mitzel, *Mod. Phys. Lett. A* **36**, 2130002 (2021).
- [2] G. Burdman, E. Golowich, J. L. Hewett, and S. Pakvasa, *Phys. Rev. D* **66**, 014009 (2002).
- [3] P. Colangelo, F. De Fazio, and F. Loporco, *Phys. Rev. D* **103**, 075019 (2021).
- [4] A. J. Buras, *Gauge Theory of Weak Decays* (Cambridge University Press, Cambridge, England, 2020).
- [5] E. Cortina Gil *et al.* (NA62 Collaboration), *J. High Energy Phys.* **06** (2021) 093.
- [6] J. K. Ahn *et al.* (KOTO Collaboration), *Phys. Rev. Lett.* **122**, 021802 (2019).
- [7] J. K. Ahn *et al.* (KOTO Collaboration), *Phys. Rev. Lett.* **126**, 121801 (2021).
- [8] P. Colangelo, F. De Fazio, P. Santorelli, and E. Scrimieri, *Phys. Lett. B* **395**, 339 (1997).
- [9] G. Buchalla, G. Hiller, and G. Isidori, *Phys. Rev. D* **63**, 014015 (2000).
- [10] W. Altmannshofer, A. J. Buras, D. M. Straub, and M. Wick, *J. High Energy Phys.* **04** (2009) 022.
- [11] P. Biancofiore, P. Colangelo, F. De Fazio, and E. Scrimieri, *Eur. Phys. J. C* **75**, 134 (2015).
- [12] A. J. Buras, J. Girrbach-Noe, C. Niehoff, and D. M. Straub, *J. High Energy Phys.* **02** (2015) 184.
- [13] L. Calibbi, A. Crivellin, and T. Ota, *Phys. Rev. Lett.* **115**, 181801 (2015).
- [14] D. Das, G. Hiller, and I. Nisandzic, *Phys. Rev. D* **95**, 073001 (2017).
- [15] M. Ahmady, A. Leger, Z. Mcintyre, A. Morrison, and R. Sandapen, *Phys. Rev. D* **98**, 053002 (2018).
- [16] S. Descotes-Genon, S. Fajfer, J. F. Kamenik, and M. Novoa-Brunet, *Phys. Lett. B* **809**, 135769 (2020).
- [17] T. E. Browder, N. G. Deshpande, R. Mandal, and R. Sinha, *Phys. Rev. D* **104**, 053007 (2021).
- [18] X. G. He and G. Valencia, *Phys. Lett. B* **821**, 136607 (2021).
- [19] R. Bause, H. Gisbert, M. Golz, and G. Hiller, arXiv: 2109.01675.
- [20] J. P. Lees *et al.* (BABAR Collaboration), *Phys. Rev. D* **87**, 112005 (2013).
- [21] T. Blake, G. Lanfranchi, and D. M. Straub, *Prog. Part. Nucl. Phys.* **92**, 50 (2017).
- [22] J. Grygier *et al.* (Belle Collaboration), *Phys. Rev. D* **96**, 091101 (2017); **97**, 099902(A) (2018).
- [23] F. Abudinén *et al.* (Belle-II Collaboration), *Phys. Rev. Lett.* **127**, 181802 (2021).
- [24] R. Bause, H. Gisbert, M. Golz, and G. Hiller, arXiv: 2007.05001.
- [25] R. Bause, H. Gisbert, M. Golz, and G. Hiller, *Phys. Rev. D* **103**, 015033 (2021).
- [26] G. Faisel, J.-Y. Su, and J. Tandean, *J. High Energy Phys.* **04** (2021) 246.
- [27] S. Fajfer and A. Novosel, *Phys. Rev. D* **104**, 015014 (2021).
- [28] L. J. Cooper, C. T. Davies, J. Harrison, J. Komijani, and M. Wingate (HPQCD Collaboration), *Phys. Rev. D* **102**, 014513 (2020).
- [29] J. Aebischer, A. Crivellin, M. Fael, and C. Greub, *J. High Energy Phys.* **05** (2016) 037.
- [30] B. Grzadkowski, M. Iskrzynski, M. Misiak, and J. Rosiek, *J. High Energy Phys.* **10** (2010) 085.
- [31] J. Fuentes-Martin, A. Greljo, J. Martin Camalich, and J. D. Ruiz-Alvarez, *J. High Energy Phys.* **11** (2020) 080.
- [32] E. E. Jenkins, M. E. Luke, A. V. Manohar, and M. J. Savage, *Nucl. Phys.* **B390**, 463 (1993).
- [33] P. Colangelo and F. De Fazio, *Phys. Rev. D* **61**, 034012 (2000).
- [34] P. Zyla *et al.* (Particle Data Group), *Prog. Theor. Exp. Phys.* **2020**, 083C01 (2020).
- [35] K. G. Chetyrkin, J. H. Kuhn, A. Maier, P. Maierhofer, P. Marquard, M. Steinhauser, and C. Sturm, *Phys. Rev. D* **96**, 116007(A) (2017).
- [36] K. G. Chetyrkin, J. H. Kuhn, A. Maier, P. Maierhofer, P. Marquard, M. Steinhauser, and C. Sturm, *Phys. Rev. D* **80**, 074010 (2009).
- [37] S. Aoki *et al.* (Flavour Lattice Averaging Group), *Eur. Phys. J. C* **80**, 113 (2020).
- [38] A. J. Buras, M. Jamin, and P. H. Weisz, *Nucl. Phys.* **B347**, 491 (1990).
- [39] J. Urban, F. Krauss, U. Jentschura, and G. Soff, *Nucl. Phys.* **B523**, 40 (1998).
- [40] F. Pisano and V. Pleitez, *Phys. Rev. D* **46**, 410 (1992).
- [41] P. H. Frampton, *Phys. Rev. Lett.* **69**, 2889 (1992).
- [42] A. J. Buras, F. De Fazio, J. Girrbach, and M. V. Carlucci, *J. High Energy Phys.* **02** (2013) 023.
- [43] A. J. Buras, F. De Fazio, and J. Girrbach, *J. High Energy Phys.* **02** (2014) 112.
- [44] A. J. Buras, F. De Fazio, and J. Girrbach-Noe, *J. High Energy Phys.* **08** (2014) 039.

- [45] A. J. Buras and F. De Fazio, *J. High Energy Phys.* **03** (2016) 010.
- [46] A. J. Buras and F. De Fazio, *J. High Energy Phys.* **08** (2016) 115.
- [47] A. J. Buras, P. Colangelo, F. De Fazio, and F. Loparco, *J. High Energy Phys.* **10** (2021) 021.
- [48] J. Brod, M. Gorbahn, and E. Stamou, *Phys. Rev. Lett.* **125**, 171803 (2020).
- [49] G. Buchalla and A. J. Buras, *Nucl. Phys.* **B412**, 106 (1994).
- [50] G. Buchalla and A. J. Buras, *Nucl. Phys.* **B548**, 309 (1999).
- [51] A. J. Buras, M. Gorbahn, U. Haisch, and U. Nierste, *Phys. Rev. Lett.* **95**, 261805 (2005).
- [52] A. J. Buras, M. Gorbahn, U. Haisch, and U. Nierste, *J. High Energy Phys.* **11** (2006) 002.
- [53] J. Brod and M. Gorbahn, *Phys. Rev. D* **78**, 034006 (2008).
- [54] J. Brod, M. Gorbahn, and E. Stamou, *Phys. Rev. D* **83**, 034030 (2011).
- [55] M. Misiak and J. Urban, *Phys. Lett. B* **451**, 161 (1999).
- [56] G. Isidori, F. Mescia, and C. Smith, *Nucl. Phys.* **B718**, 319 (2005).
- [57] F. Mescia and C. Smith, *Phys. Rev. D* **76**, 034017 (2007).